Characterizing Quantum-Dot Cellular Automata

Burkhard Ritter
Supervised by Prof. Dr. Kevin Beach

May 2014

Contents

Chapter 1

Introduction

Chapter 2

Quantum-dot cellular automata

2.1 The idea

Lent et al. introduced the concept of quantum-dot cellular automata as an alternative computing paradigm in 1993 [1]. The aim was a novel physical scheme to build digital circuits that would overcome some of the limitations of CMOS technology, promising potentially lower power consumption, higher device density, and faster clocking. As the name alludes to, quantum-dot cellular automata (QCA) is made from quantum dots which are grouped into cells. Figure 2.1(a) shows a basic QCA cell. Four quantum dots are arranged on the corners of a square. The dots are idealized as perfectly localized single orbitals on a perfectly decoupled non-intrusive medium. Therefore, each dot can be occupied by up to two electrons. In the QCA scheme, however, each cell is occupied by only two electrons in total, the cell is quarter-filled. The electrons tunnel between different dots in a cell, but the dominant energy scale has to be the Coulomb repulsion between the particles. Simply by virtue of the Coulomb repulsion, and ignoring the assumedly comparatively small tunnelling for now, the diagonal states are the two energetically preferred electron configurations as indicated in the figure. In comparison, edge states or doubly occupied quantum dots are unfavourable higher energy states, Figure 2.1(b). A priori the two diagonal states are energetically degenerate, but this degeneracy can be lifted by an external Coulomb potential, for example a second nearby QCA cell. Then these two states can be identified with logic 0 and 1, respectively.

   A single cell by itself is not very interesting. But multiple cells can be positioned next to each other, for example as a straight line of cells, Figure2.1(c). The approach now again assumes that Coulomb is the driving force and that electron tunnelling between cells is very small and ideally zero. For a straight line of cells, the long-ranging, unscreened Coulomb forces will tend to align the electron configurations of adjacent cells. If the first cell is in logic state 1 then the second cell will also prefer logic state 1 and so will in turn all the other cells in the line. The situation is the same for logic state 0. Therefore, a straight line
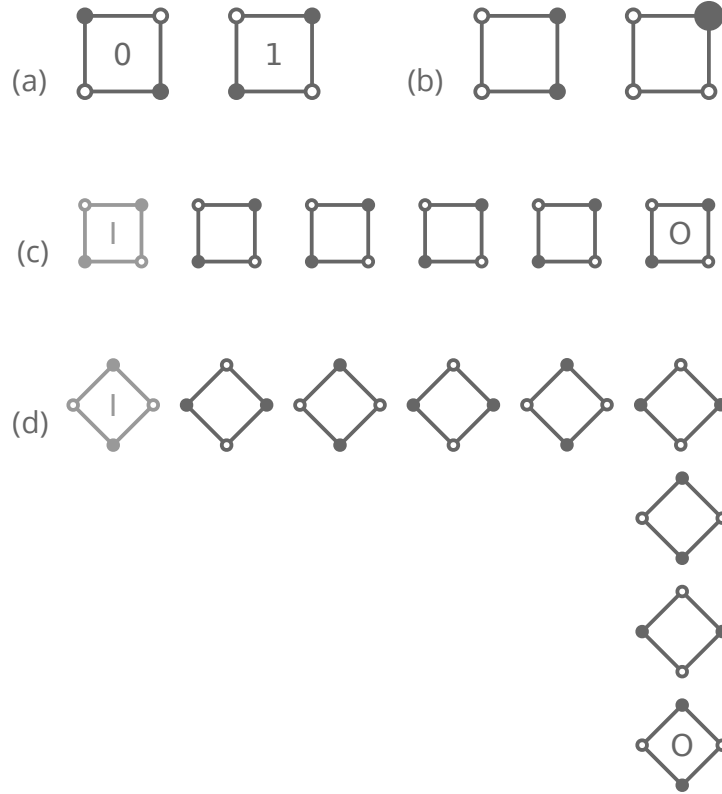
Figure 2.1: Building blocks of quantum-dot cellular automata (QCA). (a) A QCA cell consists of four quantum dots on the corners of a square and is occupied by two electrons. Due to Coulomb repulsion two energetically preferred states emerge, logic 0 and logic 1. (b) Both electrons occupying the edge of the cell or doubly occupying a single quantum dot are unfavourable high-energy states. (c) A straight line of cells functions as a wire and transmits a signal. (d) A diagonal line of cells (cells rotated by 45°) transmits a signal alternating from cell to cell. Wires can have kinks.
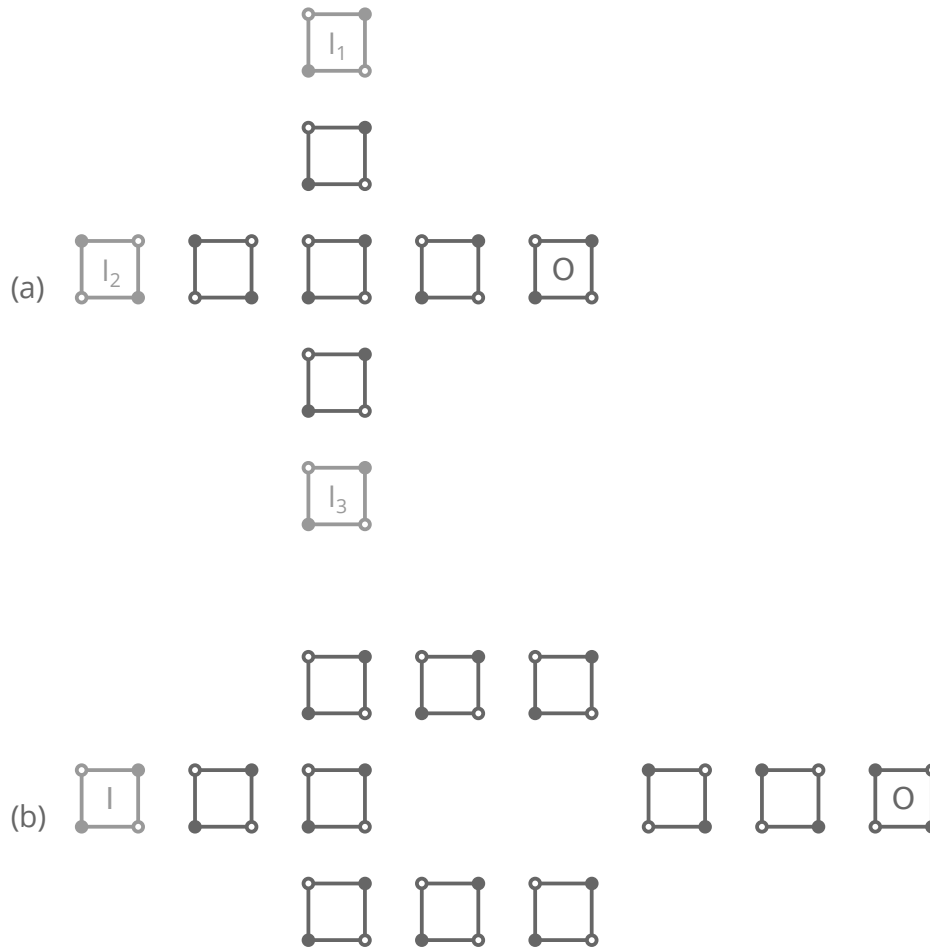
Figure 2.2: QCA gates. (a) The majority gate's three inputs "vote" on the output. The gate is commonly operated with one fixed input, for example I_3, and then functions as an AND $(I_3 = 1)$ or OR gate $(I_3 = 0)$ for the remaining two inputs. Here the gate performs the computation $1 \wedge 0 = 1$. (b) The inverter inverts a signal.

of cells is similar to a wire not only in geometry, but also in functionality: It transmits a digital signal. The same is true, with slight modifications, for a diagonal line of cells—cells rotated by 45°, Figure 2.1(d). In this case the signal alternates from cell to cell, that is, logic 1 will follow logic 0 which followed from logic 0, and this again is simply by virtue of the dominant Coulomb interaction between electrons on different cells. By using an even number of cells the diagonal line of cells works as a wire just as well as a straight line of cells. The pictogram also demonstrates a 90° kink for the diagonal line of cells which our newly gained intuition for these Coulomb-driven systems expects to pose no problem for signal transmission.

The main idea of the QCA approach becomes apparent: Ideally bistable cells interact with each other solely by Coulomb repulsion. By arranging the cells in clever geometries we can realize interesting functionalities. The idea as such is quite general and does not strictly rely on the two-electron-four-dot cell introduced above. Indeed, a number of variations exist, such as cells consisting of only two dots and occupied by only one electron, interacting via dipole fields instead of quadrupole fields as for the conventional cells. Another variation is a four-dot cell with six electrons—two holes—instead of two electrons. Even the interaction need not be Coulombic. For example, magnetic QCA schemes have been explored. While QCA carries "quantum" in its name and is sought to be implemented at the nanoscale, the approach operates close to the classical limit. The Coulomb interaction is absolutely dominating with the tunnelling of electrons a small perturbation, which nonetheless drives the system's dynamics. The approach is insensitive and in fact ignores the spin degree of freedom. Let us finally note that QCA is a not a cellular automata in a strict mathematical sense, but only by analogy to the idea of interacting cells.

One clever geometrical cell arrangement is shown in Figure 2.2(a), the majority gate. The gate has three inputs which "vote" on the central cell. The majority wins and sets the single output. The device is commonly operated with one fixed input, for example $I_3 \doteq 0$ or $I_3 \doteq 1$. In the first case, $I_3 \doteq 0$, the device functions as an AND gate for the remaining two inputs, $O = I_1 \wedge I_2$. In the second case, $I_3 \doteq 1$, it is an OR gate with $O = I_1 \vee I_2$. The figure shows the gate performing the computation $1 \wedge 0 = 1$. Now, the only missing piece for Boolean algebra is negation, $O = \neg I$. We had already seen that simply arranging cells at an 45° angle as in the diagonal line of cells negates the signal from cell to cell. The inverter, Figure 2.2(b), recasts this idea into a more robust layout. With that we have, at least in principle, all the necessary building blocks for Boolean algebra and thus digital circuitry.

Conceptually, it is most elegant to set the inputs for a QCA circuit via driver cells— cells that resemble the QCA cell in form, but are made up from static point charges instead of quantum dots. These static charges are thought to be manipulatable to vary the input smoothly from the logic 0 to the logic 1 state. In Figures 2.1 and 2.2 these driver cells are represented in light grey. Of course, in practice such driver cells would be difficult if not impossible to implement and the inputs are more likely set by leads that provide the necessary perturbative electrostatic fields. The output of a QCA device can be directly

read from its output cells. In practical implementations this will require a non-trivial charge probing apparatus. Changing the input for a QCA device throws the system into an excited, non-equilibrium state. The system will then dissipatively propagate to its new ground state. For the given inputs, this ground state corresponds to the solution of the computational problem the circuit is designed to solve. Let us emphasize this: In QCA, the computational solution maps directly to the physical ground state. During performing a computation only a few charges move locally, in each cell. Operating close to the ground state, QCA is thus a truly current-free approach and consequently inherently low-power, especially when compared with CMOS technology. But the operation close to the ground state also raises concerns for the operational temperature for these devices. It is clear that for applications we would want to engineer the system so that the energy gap between the ground state and the low-lying excited states far exceeds room temperature. Different material systems provide different dissipative channels and modelling them quantitatively or even qualitatively correctly is very challenging. As a consequence, it is difficult to derive general expectations for the clocking speed of QCA circuits. The switching speed of a majority gate, for example, will greatly depend on the system's parameters, but particularly on the nature of the dissipative coupling of the circuit to its environment. A small dissipative coupling will have the output polarization oscillating before it eventually settles to its correct value. A very dissipative system in contrast might get stuck in meta-stable states.

QCA circuits consist of wires, gates, and other structures arranged on a two-dimensional surface—very similar to conventional electronics devices. However, the structures themselves are quasi-one-dimensional and this poses a challenge for building large-scale QCA circuits. A good example is a single long wire, which is truly one-dimensional. When we think about switching the input for the wire, we think of the information being propagated as a charge density wave throughout the line of cells, or, equivalently, as propagating the domain boundary between logic 0 and logic 1. This domain boundary incurs an energy cost that the system seeks to minimize, causing the wire to order. For an increasingly longer wire, however, the gain in entropy for moving a domain boundary freely throughout the wire ($S \sim \log N$, N the number of cells) soon exceeds the loss in energy, which is reflected by the free energy of the system ($F = U - TS$). Quite generally, a one-dimensional system cannot be ordered in the thermodynamic limit except at zero temperature. Therefore, the finite-temperature infinitely long wire will always have at least two different domains, logic 0 and logic 1, and thus not be able to transmit a signal. The gap between the first excited state—with two domains—and the completely ordered ground state, together with the desired operational temperature will determine the maximum system size.

To address this scaling problem we partition large circuits into smaller units. The size of each unit is chosen to be small enough to avoid entropy-induced disorder at a given operational temperature. Each unit can be turned "on" and "off" separately: Ideally, individual gates would allow to effectively raise and lower the tunnelling barriers between quantum dots in each unit and thus allow to freeze or delocalize the electrons. A unit with
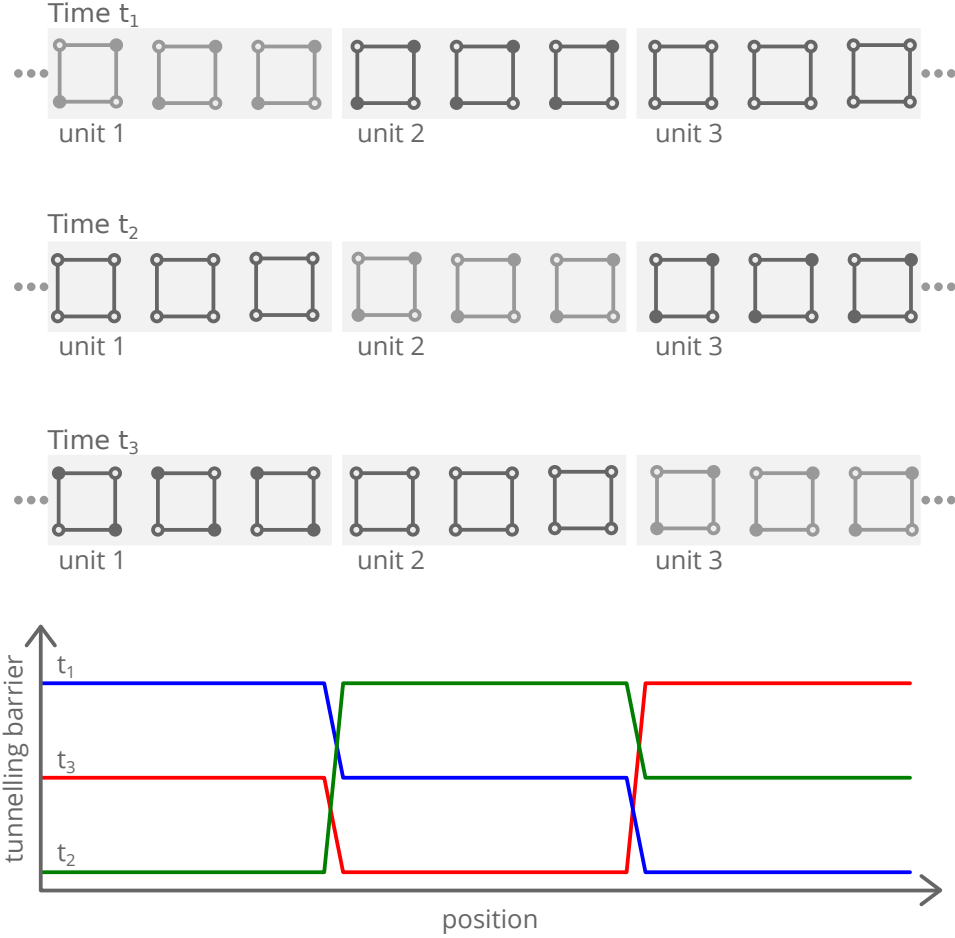
Figure 2.3: Clocked QCA for a line of cells. To avoid entropy-induced disorder in large QCA circuits, the system is partitioned into smaller units: unit 1, 2, and 3 in this example. By varying the tunnelling barriers, each unit is put through the three phases *frozen* (high barrier, light grey cells), *active* (medium barrier, dark grey cells), and *delocalized* (low barrier, dark grey cells with empty dots). Synchronizing the phases of adjacent units allows to pipeline information flow and computations. The line of cell's three units and their tunnelling barriers are shown at three different times, $t_1 < t_2 < t_3$. A logic 1 state is propagated from the left to the right. At t_3 a logic 0 state is coming in from the left.

frozen electrons can serve as the input for a unit with more *active* charge carriers, which works like a regular QCA circuit. A unit with completely *delocalized* electrons, in contrast, will not influence adjacent units. By putting each unit through the three phases *delocalized*, *active*, and *frozen* and synchronizing adjacent units appropriately, we can control the information flow through the system very nicely, as illustrated in Figure 2.3. Therefore, by partition the circuit and introducing a clocking scheme we not only handle the scaling problem, but also arrive at a pipelining architecture. If and how the tunnelling barriers can be effectively modified will depend on the details of the specific QCA implementation. Also, in practice the QCA circuit units cannot be too small as they must be individually addressable. Gates which turn QCA units "on" and "off" provide another potential benefit as well. We are able to control how and especially how fast the gate voltage is changed and should be able to tune it with respect to the inherent time-scales of the QCA system, which are set by the system's parameters and the dissipative coupling to its environment. This should afford a better control over the dynamics of the switching process and might help mitigate problems like oscillating outputs and meta-stable states, mentioned above [2].

2.2 Atomic silicon quantum dots

Our objective is the general, not implementation-specific characterization of the QCA approach. Even so it is still important to consider concrete experimental realizations, not only as a motivation for our work, but also to put our modelling and results into context. One of the most promising and recent experimental implementations of QCA is based on atomic silicon quantum dots and we will therefore use them as our experimental reference. Atomic silicon quantum dots were first demonstrated as a possible QCA implementation by Wolkow et al. in 2009, when the group realized one single QCA cell. Figure 2.4(a) shows a scanning tunnelling microscope (STM) image of this cell. Since then impressive advances have been made both in the understanding of the electronic properties of these quantum dots as well as in the precise fabrication of larger QCA structures. With atomic-scale feature sizes this experimental system promises room temperature operation, while at the same time tapping into the established and highly sophisticated silicon technology. Being based on silicon should also ease integration with existing CMOS circuitry.

Atomic silicon quantum dots are *dangling bonds* on a hydrogen-terminated (100) silicon surface. Atoms on a (100) silicon surface have two unsatisfied bonds. Pairs of surface atoms form dimers, satisfying one bond. The remaining bond is satisfied by passivating the surface with hydrogen. Figure 2.4(c) shows a STM image of the reconstructed silicon surface, where the dimer rows are clearly visible and the dimensions are indicated. By applying a relatively large current through the STM tip, individual hydrogen atoms can be removed, with atomic precision. This leaves a *dangling bond* (DB) which acts as a quantum dot: Energetically, electrons on the DB orbital sit in the silicon band gap and are therefore decoupled from the silicon substrate. Figure 2.4(b) shows the band diagram
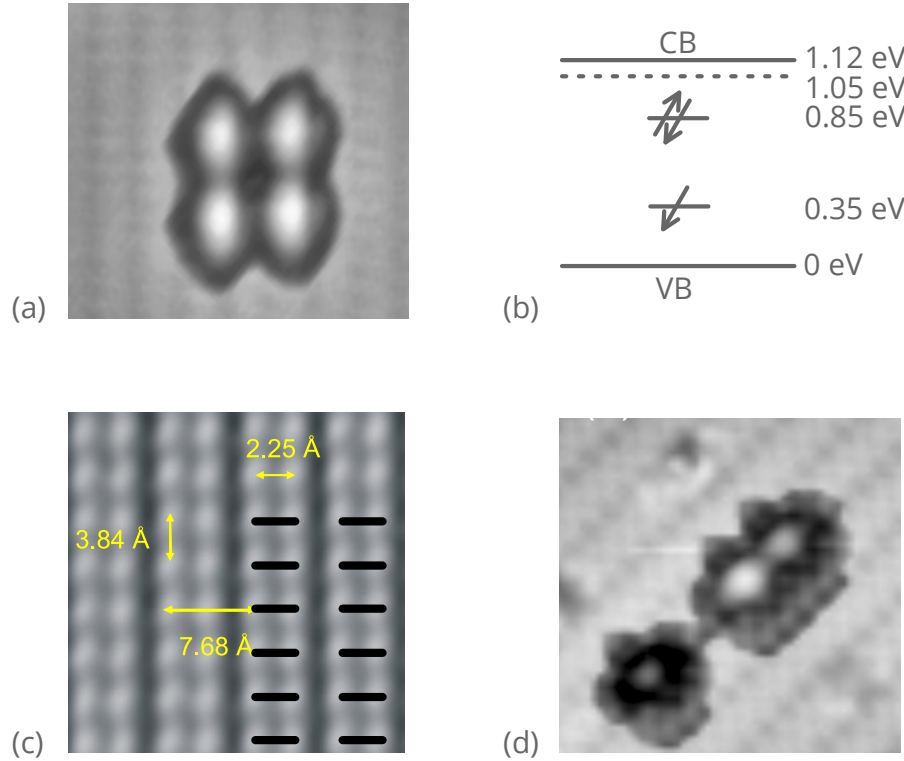
(a)

(b)

(c)

(d)

Figure 2.4: Atomic silicon quantum dots are *dangling bonds* (DBs) on a hydrogenated (100) silicon surface. (a) A scanning tunnelling microscope (STM) image of an atomic silicon quantum dot QCA cell. (b) Band diagram of a DB on a strongly n-doped silicon substrate. (c) The reconstructed (100) hydrogenated silicon surface, showing dimer rows. (d) Two closely spaced tunnel-coupled DBs perturbed by a third DB. The top right DB is seen to be more negatively charged than the other DB of the closely spaced pair, due to Coulomb repulsion from the perturbing third DB in the bottom left. All STM images and *ab initio* estimates from Wolkow et al. [3] [4].

of a DB on a n-doped substrate. Chemically, DBs have proven to be surprisingly robust with respect to environmental molecules. From *ab initio* calculations it is known that the sp^3 DB orbital extends predominantly into the bulk and only a little into the vacuum. The orbital's lateral extent is on the order of 1nm and therefore spans multiple silicon lattice atoms. Due to orbital overlap, closely spaced DBs are tunnel-coupled. A neutral DB consists of the positive silicon ion and one electron. In the experimentally common strongly n-doped system, the DB accepts one more electron and is therefore $-1e$ negatively charged. Conversely, in a p-doped sytem the DB will donate its electron and become $+1e$ positively charged. The Coulomb repulsion between negatively charged DBs can be used to adjust the filling of DB assemblies simply by the DBs' positions. For example, on a n-doped substrate two DBs may eject one electron (which goes back to the bulk) and share the remaining single electron, when placed close enough together. To proof this, a third DB is placed close by, but not close enough to be tunnel-coupled. The effect of the Coulomb repulsion can be seen via STM imaging, Figure 2.4(d), where the DB farthest from the perturbing external charge is more negatively charged (darker in the STM image) than the closer DB. The observed charge shift is only possible when both closely-spaced DBs share a single electron. To form the previously shown QCA cell, Figure 2.4(a), on a strongly n-doped silicon substrate four DBs are brought close enough together so that two electrons go back to the bulk, leaving the cell with six electrons (two holes) in total and a cell net charge of $-2e$—the right charge regime for QCA.

Atomic silicon quantum dots provide some examples of how a real world system might be different from the idealized picture we typically employ to describe the QCA approach. We like to think of quantum dots as perfectly localized orbitals. But in the silicon system the orbitals of the DBs actually span multiple lattice sites and only if the DBs are placed far enough apart might we still be able to consider them as localized. We do not consider the substrate but treat quantum dots as perfectly isolated entities. Of course, in practice the substrate will certainly influence the QCA device. In the silicon system free charge carriers will screen the long-ranged Coulomb interactions that the QCA scheme relies on. The screening is not necessarily disruptive for QCA and might even be beneficial, for example by minimizing charge-buildup in large systems. But to quantify the screening accurately it is necessary to thoroughly understand and precisely model the system in detail which, for atomic silicon quantum dots which live at the surface, would surely be very challenging. The silicon substrate could also, conceivable, provide a second tunnelling channel between DBs. In addition to electrons hopping directly from DB to DB they could first tunnel from the first DB to the substrate and then back to the second DB. Therefore an accurate model for atomic silicon quantum dots might need to accommodate the nature of the DB orbitals, screening, multiple tunnelling channels and possibly other effects.

2.3   The extended Hubbard model

QCA systems are typically modelled by an extended Hubbard Hamiltonian. The Hubbard model originated in the early 1960s to describe rare-earth systems with highly localized d- and f-electrons and has since then, of course, become one of the most widely studied and successful models in condensed matter physics [5]. In basing our description on the Hubbard model we already put some key assumptions in place. For example, we assume that the quantum dots are similar to the highly localized d-orbitals. As discussed above, depending on the particular QCA implementation this might or might not be a good description. However, our interest is not in the precise details of any particular material system QCA might be implemented on, but our aim is to investigate universal characteristics of QCA systems. An idealized but semi-realistic description is what we want and for that the Hubbard model is indeed an appropriate—and tractable—starting point. Specifically, the Hamiltonian we use is

$$H = - \sum_{ij\sigma} t_{ij}\, c_{i\sigma}^{\dagger} c_{j\sigma} + U \sum_{i} n_{i\uparrow} n_{i\downarrow} - \mu \sum_{i\sigma} n_{i\sigma} + \sum_{i<j} V_{ij}\left(n_{i\uparrow} + n_{i\downarrow} - q\right)\left(n_{j\uparrow} + n_{j\downarrow} - q\right),$$

(2.1)

where $c_{i\sigma}^{\dagger}$ ($c_{i\sigma}$) creates (annihilates) an electron on quantum-dot i with spin σ and the particle number operator is $n_{i\sigma} = c_{i\sigma}^{\dagger} c_{i\sigma}$; t_{ij} is the overlap integral between dots i and j, U is the Hubbard on-site Coulomb repulsion, μ the chemical potential, and V_{ij} the long-ranged Coulomb interaction, which is characteristic for QCA systems. For simplicity the Coulomb term is chosen to be $V_{ij} = \frac{1}{r_{ij}}$ where r_{ij} is the distance between the two dots i and j. We also introduce the *compensation charge* q which is thought to represent a possible positive ion at each quantum dot site. This constant positive charge allows us to tune the net cell charge. For two electrons per cell, for example, $q = 0$ yields a net cell charge of $-2e$ whereas $q = \frac{1}{2}$ represents zero net cell charge, and here the cell becomes a perfect electrostatic quadrupole.

The geometric layout of the QCA system and therefore its functionality is encoded in the hopping parameter t_{ij} and the long-ranged Coulomb term V_{ij}. For the hopping parameter we usually only consider nearest-neighbour hopping t and specifically no hopping between the cells. While this constraint is not strictly necessary for QCA, it is in line with the approach's underlying idea and greatly simplifies calculations. Because the overlap integral decays exponentially with distance, as long as the distance between dots from different cells is larger then the distance between dots within one cell, the assumption will introduce only a small error. Still, this is something to keep in mind if we place cells very close to each other. Note that without inter-cell hopping we can decompose the Hamiltonian into purely Coulombic cell-cell interaction terms H_{kl}^{cc} and single cell terms H_{k}^{c} which capture the kinetics as well as the inside-cell Coulomb interactions,

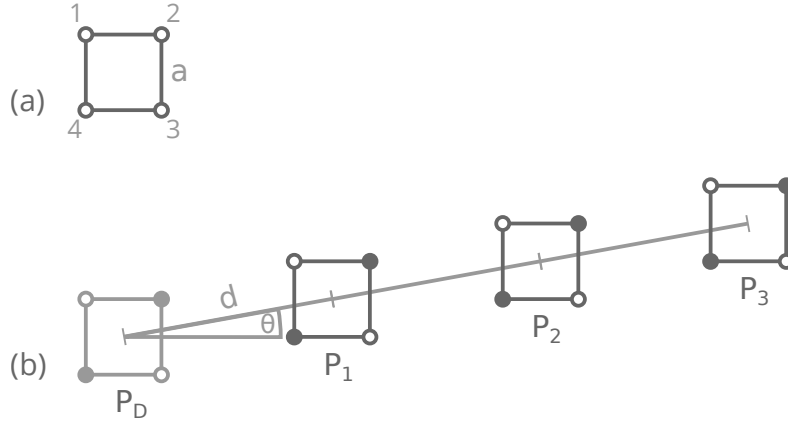$$H = - \sum_{k} H_{k}^{c} + \sum_{k<l} H_{kl}^{cc},$$

(2.2)

Figure 2.5: ...

where k and l number the cells.

To parameterize the Coulomb term V_{kl} and specifically r_{ij}, the distance between quantum-dots i and j, we introduce the cell edge length a and the cell-cell distance d, as illustrated in Fig. 2.5 where we have used a short line of cells as an example QCA system. The angle between adjacent cells is denoted by θ. Ideally each cell should be in logic state 0 or logic state 1, but, of course, in practice a cell can be in any superposition of the two states or even in a different state altogether. The *cell polarization* P_k quantifies the state of the cell,

$$P_k = \frac{1}{2}\left(n_{4k+2} + n_{4k+4} - n_{4k-1} + n_{4k-3}\right) , \tag{2.3}$$

where the dots in each cell are numbered clockwise as indicated in the figure and we have introduced the shorthand notation $n_i = n_{i\uparrow} + n_{i\downarrow}$. The cell polarization is $P_k = -1$ for a logic 0 and $P_k = +1$ for a logic 1 state. Without any external input the polarization of a cell will be $P_k = 0$. In the example line of cells, the input is set via the driver cell's polarization P_D at the left end. The driver cell's four static point charges are adjusted to reflect the desired polarization P_D. For QCA, the cell polarization really is the observable of utmost interest. It indicates whether a cell is in logic state 0 or logic state 1 and how polarized the cell is, where ideally, of course, the cell should always be fully polarized $|P_k| = 1$. In short, the cell polarizations will indicate how well the QCA approach works for a given system and, unsurprisingly, calculating cell polarizations for various geometric layouts over a wide range of system parameters will be our main focus.

The QCA cell is characterized by three energy scales: the nearest-neighbour hopping t, the nearest-neighbour Coulomb repulsion $V_1 = \frac{1}{a}$, and the on-site Coulomb repulsion U. For QCA operation U is usually assumed to be sufficiently large so that doubly occupied states are gapped out. We can introduce $V_2 = \frac{1}{\sqrt{2}a}$, the next-nearest-neighbour Coulomb repulsion, which corresponds to both electrons sitting on the diagonal of the cell—our

preferred $P = \pm 1$ states, ideally the ground state. Conversely, V_1 corresponds to both electrons occupying the edge of the cell. Again, for QCA operation we would like the edge states to be sufficiently gapped out. Therefore, the energy gap $\Delta V = V_1 - V_2 = \frac{2-\sqrt{2}}{2a} \sim 0.3V_1$ and to a lesser extent $U \gg \Delta V$ will directly determine how polarized our cell is. V_1 will thus seek to order the cell. It competes with the hopping t which delocalizes and unorders the electrons. QCA is thought to function in a regime where the ratio $\frac{V_1}{t}$ is large. Of course, it is also clear that if $\frac{V_1}{t}$ becomes too large, for example by taking $t \to 0$, the system becomes slower and eventually freezes which is also undesirable for QCA operation. To complete the picture we have to put in the temperature T, because what we really mean by saying "sufficiently gapped out" is an energy gap relatively large compared to temperature. In essence we can therefore characterize a cell by the ratios $\frac{V_1}{t}$, $\frac{U}{t}$, and T/t. By similarly expressing the cell-cell distance in units of the cell size, $\frac{d}{a} = dV_1$ we characterize any QCA system in dimensionless units.

2.4   Intercellular Hartree and two-state approximation

At the time of this writing, the QCA idea is over twenty years old. Naturally, the fundamental building blocks of QCA circuitry, such as the single cell itself, the wire, and the majority gate, have been characterized, typically numerically, but to a very limited extent also experimentally. Interestingly, time-independent properties were investigated relatively briefly and arguably not exhaustively. The bulk of the existing work soon focused on system dynamics, building large scale computing architectures with the QCA paradigm, and on specific potential experimental realizations. The characterization of time-indepentend QCA properties yielded two main results. First, the cell-cell response, that is, how the polarization of one cell responds to the polarization of a neighbouring cell, was established to be non-linear and exhibit gain [1]. Therefore, even an only partially polarized cell would fully polarize the cell next to it, Fig. 2.6(a). Of course, gain is highly desirable, if not essential, for building digital circuits. It compensates any loss or imperfections and makes the scheme overall robust. Not coincidentally, CMOS technology is built around the MOSFET transistor with gain as one of its intrinsic properties. Second, lines of cells were seen to be constantly polarized, Fig. 2.6(b) [6]. Thus, apart from few cells next to the driver cell, all remaining cells in the line would be polarized with the same polarization, the *saturation* polarization. The *saturation* polarization was observed to be largely independent of the dirver cell's polarization, but solely determined by the system's parameters such as the hopping t and the Coulomb energy V_1. For unfavourably chosen parameters the *saturation* polarization might be zero, but over a wide range of system parameters it was shown to be close to perfect. For example, for large hopping t the *saturation polarization* is expected to be zero. If t is then decreased passes a critical point t_c a first order phase transition takes place, the *saturation* polarization becomes non-zero and in fact very quickly close to perfect as t is further decreased. In addition to the cell-cell response and the analysis of a line of
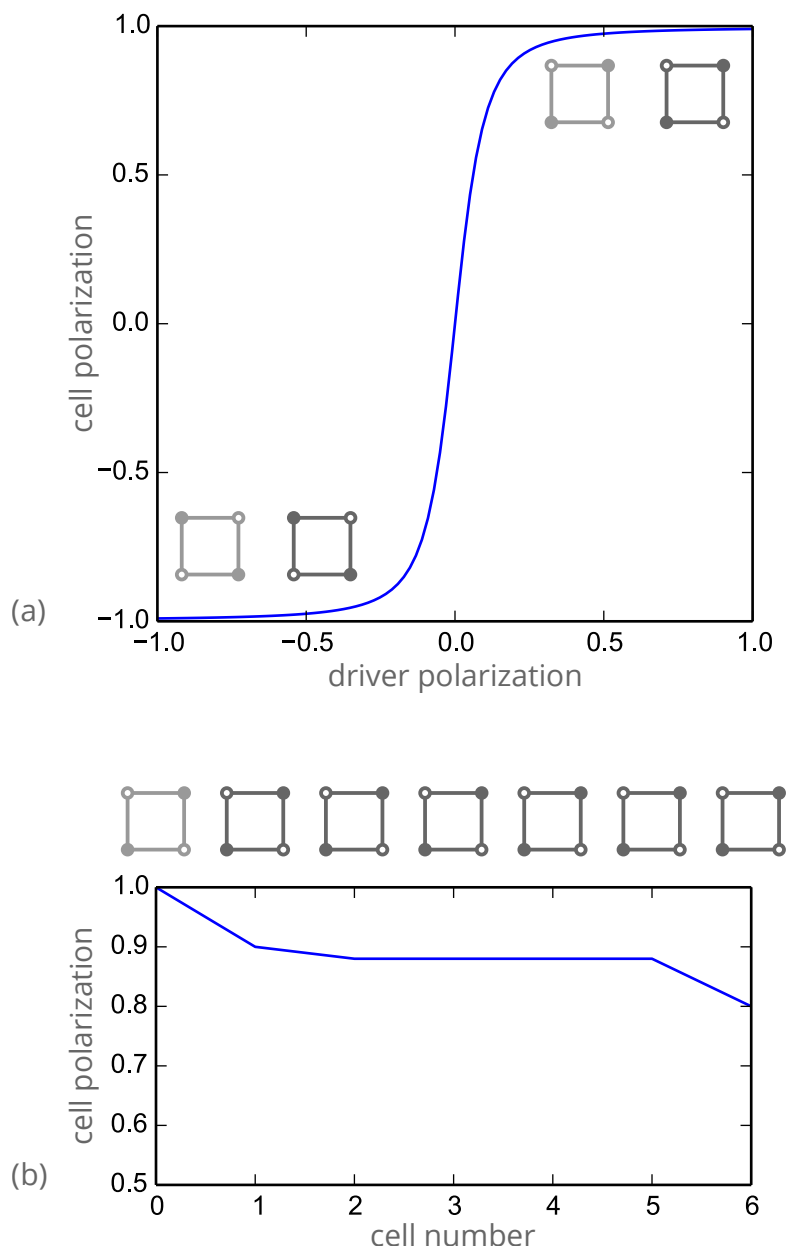
(a)

(b)

Figure 2.6: . . . ; TODO: frame of plots should be grey, not black

cells, larger QCA structures such as the majority gate were reported to function correctly for a select set of parameters, but were not analyzed in depth. Overall, the physical picture emerging from the early time-independent calculations is of bistable cells readily snapping into the correct fully polarized state throughout the whole device. It is a picture where the QCA approach works almost perfectly over a presumably wide range of parameters and it is the prevailing picture to this day. It is also quite wrong.

These early calculations of time-independent QCA properties concentrated almost exclusively (with one exception [7]) on the ground state of the system. However, focusing solely on the ground state is not sufficient. While the QCA approach is intended to be operated "close to the ground state" at least the first excited state is needed to obtain an estimate for the operational temperature for these devices—a parameter of significant practical interest. More subtly, what the QCA idea calls "ground state", ideally $P = -1$ or $P = 1$, actually corresponds to multiple states, namely, one spin singlet and three spin triplet states for $P = -1$ and $P = 1$, respectively, in a single cell. While these states can reasonably be expected to be near-degenerate, a thorough study of QCA should still consider them. In more practical terms, QCA is expected to operate at finite temperatures so simulating the devices at non-zero temperature just makes sense. Similarly, the existing work on time-independent QCA properties is not exhaustive in the exploration of other parameters. For example, while the *saturation* polarization's dependence on V_1 and t is mapped out, concrete numerical values for these quantities are hard to come by. In other cases the Coulomb scale V_1 is not indicated explicitly at all. Cells are assumed to be charge-neutral, but the effects of non-charge-neutrality is not investigated. Different cell-cell distances are not discussed, nor what system parameters should be chosen for optimal performance.

The exact numerical simulation of QCA systems is challenging and in fact intractable for all but the smallest structures. Therefore, approximations are necessary. In the literature on QCA two approximations are prevailing: The intercellular Hartree approximation (ICHA) and the two-states-per-cell approximation [1] [8]. Most of the studies of time-independent QCA properties employ the ICHA. Only the cell-cell response is calculated with a "full" quantum mechanical model, where the "full" model is actually already the reduced Hilbert space of exactly two electrons per cell. ICHA is a mean field scheme: The Hamiltonian of one cell is solved exactly in the mean field of the polarizations of all the

other cells. More specifically, the cell-cell interaction term H_{kl}^{cc} in eq. (2.2) is rewritten

$$
\begin{aligned}
H_{kl}^{cc} &= \sum_{\substack{i \in k \\ j \in l}} V_{ij} \left(n_i - q\right) \left(n_j - q\right) \\
&\sim \sum_{\substack{i \in k \\ j \in l}} V_{ij} \left[\frac{1}{2} \left(n_i - q\right) \left(\langle n_j \rangle - q\right) + \frac{1}{2} \left(\langle n_i \rangle - q\right) \left(n_j - q\right) \right] \\
&\sim \frac{1}{2} \sum_{i \in k} \left(n_i - q\right) \tilde{V}_i^l + \frac{1}{2} \sum_{j \in l} \left(n_j - q\right) \tilde{V}_j^k,
\end{aligned}
\tag{2.4}
$$

and the one-cell mean field Hamiltonian becomes

$$
H_{mf} = H^c + \sum_i \left(n_i - q\right) \left(\sum_l \tilde{V}_i^l(\langle P_l \rangle) \right). \tag{2.5}
$$

Because the cell polarization is directly related to the occupancies of the sites of the cell, we have $\tilde{V}_i^l = \tilde{V}_i^l(\langle P_l \rangle)$. Solving the one-cell Hamiltonian allows to compute to polarization $\langle P \rangle$ of the cell which in turn is used to set the mean field $\sum_l \tilde{V}_i^l(\langle P_l \rangle)$, with $\langle P_l \rangle = \langle P \rangle$, originating from all other cells. The procedure is repeated until a self-consistent cell polarization and thus self-consistent solution for Eq. (2.5) is found. By using, for example $n_i n_j \sim \frac{1}{2} n_i \langle n_j \rangle + \frac{1}{2} \langle n_i \rangle n_j$, mean field approximations neglect quantum fluctuations. Only at high dimensionality can these fluctuations really average to zero and indeed mean field schemes can be shown to become exact in the limit of infinite dimensionality [9]. Conversely, for low dimensional systems fluctuations are more important and mean field approximations are intuitively expected not to work very well. As uncontrolled approximations the validity of mean field approaches needs to be verified on a case by case basis. Because QCA is quasi-one-dimensional it is arguably not well-suited for a mean field treatment. Even then a mean field approximation might be appropriate as a first stab at the problem. However, the infinite wire discussed above provides a simple example where ICHA already goes wrong. We argued that due to entropy the infinite wire can only be ordered at zero temperature. In contrast, a mean field approximiation will predict order up to a finite critical temperature. ICHA was introduced in the very first QCA paper. The approximation was never verified or complemented by more accurate methods. It is rather remarkable that a large part of the existing work on QCA characterization rests, directly or indirectly, on an approximation that can reasonably be expected to give wrong results. And indeed, in the context of the dynamic properties of QCA it has been known for a long time that ICHA gives qualitatively wrong results [10]. Much more recently, it has been shown very explicitly that even for the single cell-cell response ICHA introduces artifacts that are clearly non-physical [11].

For the calculation of time-dependent properties the two-states-per-cell approximation is typically used, precisely because it was realized that ICHA does give wrong results, for

example for the switching behaviour of some majority gate structures. Perplexingly, in the literature the two-state approximation is motivated and justified by the ICHA picture [8]. Starting from the observation that wires are polarized with a *saturation* polarization (in ICHA calculations), a cell is represented by two basis states, corresponding to $P = P_{sat}$ and $P = -P_{sat}$. In a loose sense, the two-states-per-cell model thus comes from a picture of how we would like QCA to work: Perfectly bistable, interacting cells. The approximation has been verified to the extent that it was shown that the ground state of the full quantum mechanical model can be represented nearly perfectly by the two-state basis, but only for one cell and for one particular set of system parameters. In a more rigorous treatment it should be possible to clearly derive the two-state model as the correct emerging low-energy Hamiltonian from the original extended Hubbard model. Such a derivation would also work out the parameter regime where the effective two-state Hamiltonian is valid. We will attempt it in due course. In contrast to ICHA the two-states-per-cell approximation retains inter-cell entanglement and therefore yields more correct results, not only for dynamics, but also for time-independent properties. As the price the two-state model scales exponentially, whereas ICHA scales linearly in system size. Therefore, even with the two-state approximation only relatively small QCA devices are computationaly feasible. As a last note, the two-state model is clearly very similar to a transverse field quantum Ising model, where the two polarization states correspond to a pseudo spin and the hopping is like a transverse field, flipping the cell polarizations.

2.5   Exact diagonalization

We use the exact diagonalization numerical method [9] to simulate QCA systems described by the Hamiltonian (2.1). In principle, exact diagonalization is a straightforward method: For a chosen basis the matrix of the Hamiltonian is constructed explicitly and then diagonalized, yielding the eigenenergies and eigenstates of the system. With that we know everything about the system and can calculate observables of interest. The problem is that memory consumption scales as N_s^2 and the computational cost roughly as N_s^3, where N_s is the size of the state space; and the number of states scales exponentially with system size, $N_s = 4^{N_d} = 256^{N_c}$. N_d denotes the number of dots and N_c the number of cells. As an example, to store the full Hamiltonian matrix of a two cell QCA system requires 3GB of memory, to store the Hamiltonian matrix of a three cell system already requires 2000TB. That's clearly not feasible on any available computer. As a side note, we cannot employ projective algorithms like Lanczos [9], because we are interested in finite temperatures and therefore need the full energy spectrum. Typically, projective schemes are only useful to calculate the ground state or the few lowest energy states.

    To decrease the memory requirements and computational cost of exact diagonalization symmetries must be exploited. The Hamiltonian matrix is actually quite sparse—most entries are zero. By using symmetries and a suitable basis the Hamiltonian matrix can

be brought into block diagonal form and then only those much smaller blocks need to be diagonalized. Our QCA system is symmetric with respect to the total particle number $\hat{N} = \sum_i \hat{n}_{i\uparrow} + \hat{n}_{i\downarrow}$ and the total spin $\hat{S} = \sum_i \hat{n}_{i\uparrow} - \hat{n}_{i\downarrow}$, i.e. $[\hat{N}, \hat{H}]_- = [\hat{S}, \hat{H}]_- = 0$. If we now use basis states which are eigenstates of the symmetry operators, $|n, s, l\rangle$, with

$$
\begin{aligned}
\hat{N} \, |n, s, l\rangle &= n \, |n, s, l\rangle \ , \\
\hat{S} \, |n, s, l\rangle &= s \, |n, s, l\rangle \ ,
\end{aligned}
\tag{2.6}
$$

then we have

$$
\begin{aligned}
\langle n', s', l' | \, [\hat{N}, \hat{H}]_- \, || n, s, l\rangle &= (n' - n) \, \langle n', s', l' | \, \hat{H} \, |n, s, l\rangle \overset{!}{=} 0 \\
\langle n', s', l' | \, [\hat{S}, \hat{H}]_- \, |n, s, l\rangle &= (s' - s) \, \langle n', s', l' | \, \hat{H} \, |n, s, l\rangle \overset{!}{=} 0
\end{aligned}
\tag{2.7}
$$

and therefore

$$
\langle n', s', l' | \, \hat{H} \, |n, s, l\rangle = 0 \qquad \text{for } n \neq n' \text{ or } s \neq s' \, .
\tag{2.8}
$$

Consequently, by ordering basis states by the symmetry operators' eigenvalues the Hamiltonian matrix becomes block diagonal, where the blocks are labelled by n and s. The blocks can be constructed and diagonalized separately and all observables can then be calculated block-wise as well, hence vastly reducing memory requirements and computational time. In our implementation, however, we do keep all blocks in memory simultaneously. This still yields considerably reduced memory usage and the same speedup in computational time. For the QCA system the single largest block is the spin zero sector at half-filling. Its size is

$$
N'_s = \binom{N_d}{\frac{1}{2}N_d}^2 .
\tag{2.9}
$$

This corresponds to memory requirements of 180MB for two cells and 5400GB for three cells. Thus, although this is a considerable improvement for the two cell system (not least in computational time), the three cell system still remains unreachable with conventional computer hardware. To access larger systems we need to introduce approximations, which we will pursue in detail and with great care in the following chapter.

Computational physics is, true to its name, to considerable extent concerned with writing computer code. If ingenious algorithms which bring sophisticated physical problems to the computer are the art that excites the computational physicist's intellect, then writing good computer code is the craft. It is a curious fact that traditionally in computational condensed matter physics little weight has been put on coding techniques, collaboration on the code level, and the code itself. This not only frustrates the newcomer to the field, for it is a long way from a formally stated algorithm to a correct and efficient implementation, but also poses a more fundamental problem to science in a time when computing has long become an essential part of it. Scientific results obtained from sophisticated numerical algorithms can be difficult to verify and reproduce without an openly available implementation

of those algorithms. But verification and reproducibility are core assets of the scientific process. Fortunately, the culture is slowly changing. In computational condensed matter physics, the ALPS and Abinit projects provide open implementations of a variety of commonly used methods and algorithms [12] [13]. In the wider scientific community, IPython is a shining example of building a powerful computational tool collaboratively, with a huge impact across disciplines [14].

Our QCA exact diagonalization implementation is written in C++ and uses the excellent Eigen linear algebra library [15]. Matrices are stored in sparse representation, except for the block-wise diagonalization itself, performed by Eigen, where we use dense matrices. The basis states can be filtered and sorted, e.g. to truncate the Hilbert space to a specific charge sector and to exploit symmetries. We do not build the Hamiltonian matrix directly, but instead construct creation and annihilation operator matrices. Therefore, operators such as the Hamiltonian and the polarization can be expressed in an intuitive, almost mathematical notation. We employ the curiously recurring template pattern to achieve simple static polymorphism, avoiding the overhead of runtime polymorphism [16]. In less abstract terms, this allows us to reuse code, for example the Hamiltonian, for the conceptually similar, but physically quite different various QCA models which we are going to introduce in detail in the next chapter. Our C++ code cannot be executed directly, but is instead compiled as an extension module for the Python language, via the Boost library's Boost.Python [17]. We also use the unit testing framework from the Boost library. In our experience, making the C++ code available in Python provides enormous benefits. With Python data input, output and storage becomes a breeze, especially compared to the chore these tasks are in pure C++. Python makes it easy to script and distribute (i.e. simply parallelize) simulation runs, and, being well established in the scientific community, comes with extensive libraries for data analysis and plotting, e.g. SciPy and Matplotlib [18] [19]. Consequently, the integration with Python facilitates quickly trying out new ideas, implementing new features and more fluid data analysis. The advent of the fantastic IPython notebook ties all of these pieces together in a consistent, productive and highly enjoyable workflow [14]. The IPython notebook is also an apt format for effectively communicating results with colleagues. The disadvantages of the Python integration are the additional dependencies, although both Python and Boost are commonly available on any number of platforms these days, and the more involved (and hence error-prone) build process. We have written a small Python library to support our data storage and organization needs. The library facilitates storing and retrieving data in standard file formats and allows to define and run "numerical experiments," which can be distributed across multiple computers. Both the QCA exact diagonalization code and the Python library are available under an open license on GitHub [20] [21].

Chapter 3

Approximations

Bibliography

[1] C. S. Lent, P. D. Tougaw, W. Porod, and G. H. Bernstein, "Quantum cellular automata," *Nanotechnology* **4** (1993) 49.

[2] C. S. Lent and P. D. Tougaw, "A device architecture for computing with quantum dots," *Proceedings of the IEEE* **85** (1997) 541–557.

[3] R. A. Wolkow, L. Livadaru, J. Pitters, M. Taucer, P. Piva, M. Salomons, M. Cloutier, and B. V. C. Martins, "Silicon Atomic Quantum Dots Enable Beyond-CMOS Electronics," *arXiv preprint arXiv:1310.4148* (2013) .

[4] J. L. Pitters, L. Livadaru, M. B. Haider, and R. A. Wolkow, "Tunnel coupled dangling bond structures on hydrogen terminated silicon surfaces," *The Journal of chemical physics* **134** (2011) 064712.

[5] J. Hubbard, "Electron correlations in narrow energy bands. III. An improved solution," *Proceedings of the Royal Society of London. Series A. Mathematical and Physical Sciences* **281** (1964) 401–419.

[6] C. S. Lent and P. D. Tougaw, "Lines of interacting quantum-dot cells: A binary wire," *Journal of Applied Physics* **74** (1993) 6227–6233.

[7] P. D. Tougaw, C. S. Lent, and W. Porod, "Bistable saturation in coupled quantum-dot cells," *Journal of Applied Physics* **74** (1993) 3558–3566.

[8] P. D. Tougaw and C. S. Lent, "Dynamic behavior of quantum cellular automata," *Journal of Applied Physics* **80** (1996) 4722–4736.

[9] H. Fehske, R. Schneider, and A. Weiße, *Computational Many-Particle Physics*. Lecture Notes in Physics. Springer, 2008. http://books.google.ca/books?id=XlQIFiSk7A8C.

[10] G. Tóth and C. S. Lent, "Role of correlation in the operation of quantum-dot cellular automata," *Journal of Applied Physics* **89** (2001) 7943–7953.

[11] M. Taucer, F. Karim, K. Walus, and R. A. Wolkow, "Consequences of many-cell correlations in treating clocked quantum-dot cellular automata circuits," *arXiv preprint arXiv:1207.7008* (2012) .

[12] B. Bauer, L. Carr, H. Evertz, A. Feiguin, J. Freire, S. Fuchs, L. Gamper, J. Gukelberger, E. Gull, S. Guertler, *et al.*, "The ALPS project release 2.0: open source software for strongly correlated systems," *Journal of Statistical Mechanics: Theory and Experiment* **2011** (2011) P05001.

[13] X. Gonze, B. Amadon, P.-M. Anglade, J.-M. Beuken, F. Bottin, P. Boulanger, F. Bruneval, D. Caliste, R. Caracas, M. Cote, *et al.*, "ABINIT: First-principles approach to material and nanosystem properties," *Computer Physics Communications* **180** (2009) 2582–2615.

[14] F. Perez and B. E. Granger, "IPython: a system for interactive scientific computing," *Computing in Science & Engineering* **9** (2007) 21–29.

[15] G. Guennebaud, B. Jacob, *et al.*, "Eigen v3." Http://eigen.tuxfamily.org, 2010.

[16] A. Alexandrescu, "Modern C++ design: generic programming and design patterns applied,".

[17] "Boost C++ Libraries." `http://www.boost.org`.

[18] E. Jones, T. Oliphant, P. Peterson, *et al.*, "SciPy: Open source scientific tools for Python," 2001–. `http://www.scipy.org/`.

[19] J. D. Hunter, "Matplotlib: A 2D graphics environment," *Computing in Science & Engineering* **9** (2007) 0090–95.

[20] B. Ritter, "QCA TODO," 2014.

[21] B. Ritter, "Coma: A small Python library aiding with some aspects of running computer simulations," 2014. `https://github.com/meznom/coma`.